Electronic Supplementary Material (ESI) for Chemical Science.

Supporting Information

Diachronic Evolvement from Tetra-Icosahedral to Quasi-Hexagonal Close-Packed Bimetal Clusters

Shisi Tang,[#,a] Endong Wang,[#,b] Yanzhen Wu,[#,c] Tongxin Song,[a] Meng Zhou,[*,c] Xiao Cai,[a] Yi Gao,[*,b] Weiping Ding,[a] and Yan Zhu[*,a]

[a]School of Chemistry and Chemical Engineering, Nanjing University, Nanjing 210093, China

[b]Phonon Science Research Center for Carbon Dioxide, Shanghai Advanced Research Institute, Chinese Academy of Sciences, Shanghai 201210, China

[c]Hefei National Research Center for Physical Sciences at the Microscale, Department of Chemical Physics, University of Science and Technology of China, Hefei 230026, China

*Corresponding authors: Yan Zhu: zhuyan@nju.edu.cn; Yi Gao: gaoyi@sari.ac.cn; Meng Zhou: mzhou88@ustc.edu.cn.

1. Experimental section

Synthesis of AuC≡CR (R = 2,4-2CH_3-C_6H_3)

1 g (Me_2SAu)Cl and 60 mL acetone were added into 150 mL flask. After (Me_2SAu)Cl fully dissolving, 800 μL 1-ethynyl-2,4-dimethylbenzene was added successively under vigorously stirring and the clear solution immediately became cloudy. Then 603 μL triethylamine was added, the suspension immediately turned to clear orange solution. The reaction was carried out in the dark at room temperature for 2 hours. The solvent was removed by rotary evaporation, and the remaining orange solid was washed with water, ethanol and ether in turn to remove the excess alkyne. Finally, after dried in an atmosphere of nitrogen, yellow powder was obtained.

Synthesis of AgC≡CR (R = 2,4-2CH_3-C_6H_3)

1 g $AgNO_3$ was added in 20 mL concentrated ammonia water slowly under ice bath condition. After about 5 minutes of stirring, the Tollens' reagent was obtained by filtered the solution. 650 μL 1-ethynyl-2,4-dimethylbenzene dissolved in 2 mL ethanol then was added to Tollens' reagent, generating the flaxen turbid fluid immediately. After that, the reaction solution was centrifuged and the centrifugate precipitate was washed with water, ethanol and diethyl ether to remove the excess alkyne. Finally, after dried in an atmosphere of nitrogen, flaxen powder was obtained.

Synthesis of $Au_{30}Ag_{12}$(C≡CR)$_{24}$ nanocluster: $Au_{30}Ag_{12}$(C≡CR)$_{24}$ was synthesized by the direct reduction of the AuC≡CR and AgC≡CR (R = 2,4-2CH_3-C_6H_3) (See Supporting Information for synthesis methods) precursor with tert-butylamine borane ($C_4H_{11}NBH_3$). Firstly, AuC≡CR and AgC≡CR were synthesized as described above. Then 60 mg AuC≡CR and 28 mg AgC≡CR were added into a 50 mL flask containing mixture of dichloromethane and methanol under vigorously stirring. When the solution turned turbid orange, 1.0 mg $C_4H_{11}NBH_3$ was added. The reaction was carried out for 12 hours at room temperature. Then the reaction solution was centrifuged and the sediment was discarded. To remove excess alkynes and reductants, the supernatant was washed several times with methanol, and then was extracted with dichloromethane to obtain crude product. The crude product was separated and purified by thin layer chromatography with dichloromethane/petroleum ether as chromogenic agent. Finally, the light green product was extracted by dichloromethane and layered with n-hexane for 10 days to obtained $Au_{30}Ag_{12}(C\equiv CR)_{24}$ single crystal (crystal data and structure refinement for the $Au_{30}Ag_{12}(C\equiv CR)_{24}$ nanoclusters is shown in Table S1).

Conversion from $Au_{30}Ag_{12}(C\equiv CR)_{24}$ to $Au_{47}Ag_{19}(C\equiv CR)_{32}$: 2 mg pure $Au_{30}Ag_{12}(C\equiv CR)_{24}$ was dissolved in 4 mL CH_2Cl_2, and then 0.5 mg $C_4H_{11}NBH_3$ dissovled in CH_3OH was added under vigorously stirring. Then the reaction was carried out for about 108 h and the color of the solution slowly changed from green to burgundy. Then the reaction liquid was centrifuged and the supernatant was $Au_{47}Ag_{19}$ crude product. Finally, the amaranth product was extracted by dichloromethane and layered with n-hexane for 10 days to obtained $Au_{47}Ag_{19}(C\equiv CR)_{32}$ single crystal (crystal data and structure refinement for the $Au_{47}Ag_{19}(C\equiv CR)_{32}$ nanoclusters is shown in Table S2).

Catalytic tests

All electrochemical tests were implemented on the electrochemical workstation CHI660D using a standard three-electrode system with glassy carbon electrode (GCE) (diameter: 5 mm, area: 0.196 cm^2) as the working electrode, platinum wire as the counter electrode, and Ag/AgCl as the reference electrode. The obtained nanoclusters and multiwalled carbon nanotube were added into CH_2Cl_2. After the turbid liquid was treated under ultrasonication for 30 min, the solvent was removed to obtain supported catalysts. The catalyst was dispersed in a mixture containing isopropanol, ultrapure water and 0.5 wt% Nafion solution to prepare a 0.48 mg_{AuAg}/mL catalyst suspension. Then, 2.5 μL suspensions of nanoclusters on multiwalled carbon nanotube (0.48 mg_{AuAg}/mL) were dropped on the GC electrode and then dried at room temperature. The electrocatalytic EOR performance was determined by cyclic voltammograms (CVs) conducted in a mixture solution of 1.0 M KOH and 1.0 M C_2H_5OH from -0.6 to 0.6 V vs Ag/AgCl with a sweep rate of 50 mV/s at room temperature.

Characterization

The UV−vis spectra were characterized by a Shimadzu UV-1800 UV−vis spectrometer. The single crystal X-ray diffraction data of $Au_{30}Ag_{12}(C\equiv CR)_{24}$ and $Au_{47}Ag_{19}(C\equiv CR)_{32}$ were collected on a Bruker D8 VENTURE with Mo Kα radiation (λ = 0.71073 Å) at 296 K. Electrospray ionization (ESI) mass spectra of $Au_{30}Ag_{12}(C\equiv CR)_{24}$ were collected using a Z spray source on a Waters Q-TOF mass spectrometer. The cluster sample was dissolved in toluene (0.5

mg/mL) and then the solution was diluted with methanol solution containing 50 mmol/L Cs_2CO_3 (2:1 v/v). Chemical compositions of the $Au_{47}Ag_{19}(C\equiv CR)_{32}$ was determined by matrix-assisted laser desorption ionization time of flight (MALDI-TOF) mass spectrometry in positive-ion mode with trans-2-[3-(4-tert-Butylphenyl)-2-methyl-2-propenylidene] malononitrile (DCTB) as the matrix. Electrochemical impedance spectroscopy (EIS) tests were carried out on the electrochemical workstation CHI660D using a standard three-electrode system with glassy carbon electrode as the working electrode, platinum wire as the counter electrode, and Ag/AgCl as the reference electrode. The electrolyte was 1.0 M KOH + 1.0 M C_2H_5OH, and the EIS tests were carried out at room temperature. The liquid products were determined by ^1H NMR on BRUKER AVANCE III 400 MHz with Dimethyl sulfoxide (DMSO) as internal standard. The CO_3^{2-} in EOR products was detected by ion chromatograph on Dionex Aquion equipped with Dionex IonPac AS19 column. The electrochemically active surface areas (ECSAs) were determined by integrating the hydrogen adsorption charge on CVs, which was conducted in a 1.0 M KOH solution with a sweep rate of 50 mV/s under room temperature.

Femtosecond and nanosecond transient absorption spectroscopy

We used a home-built transient absorption spectrometer to measure the femtosecond TA spectra at different time delays. The fs-TA setup is built based on a Ti: sapphire laser system (Coherent, 800 nm, 35 fs, 7.5 mJ, 1 kHz). The tunable pump pulse was generated by a commercial collinear optical parametric amplifier (LightConversion). A small portion of the fundamental 800 nm was focused on a sapphire (Eskma) to generate while supercontinuum in the visible range (420-850 nm). The pump and probe overlapped in time and space. The time delay between the pump and the probe pulse is varied between -1 ps and 2000 ps using a retroreflector mounted on a mechanical delay state (DL325, Newport). The transient absorption spectra were obtained using dual spectrometers with a data rate of 2k (2048CL, Avantes). All measurements were performed in diluted solution of toluene. Nanosecond transient absorption measurements were conducted using the same ultrafast pump pulses along with an electronically delayed supercontinuum light source with a sub-nanosecond pulse duration (Nano100, Time-Tech Spectra).

2. Computational details

Density functional theory (DFT) calculation was applied. Perdew-Burke-Erzerho GGA functional was employed throughout all the calculations of this work. Effective-core basis set

LANL2DZ was chosen for Au and Ag atoms. The rest atoms including C, O, and H were described by using 6-31G(d) basis set. All the organic ligands were replaced by –H to reduce the computational price. Calculations on catalytic mechanism were performed with Gaussian 09-D01 package.[S1] Structural transformation from $Au_{30}Ag_{12}$ to $Au_{47}Ag_{19}$ and super-fast approximate TD-DFT by Grimme and co-workers to get the UV-abs spectrum were performed via the Orca 5.0.3 package.[S2,S3] To show how the Gibbs free energy was obtained, the following H removal reaction was taken as example.

$$CH_3CH_2OH@cluster + OH^{-} \rightarrow CH_3CH_2OH@cluster + e^{-} + H_2O \qquad (1)$$

At neutral pH, $H_2O(l) \rightleftharpoons H^+(aq) + OH^-(aq)$. Previous study[S4] suggested that the OH^- can be substituted through $H_2O(l)$ - $H^+(aq)$ leading to equation (2). These equations are equivalent from the thermodynamic perspective.

$$CH_3CH_2OH@cluster \rightarrow CH_3CH_2OH@cluster + e^{-} + H^{+} \qquad (2)$$

Then, the Gibbs free energy was obtained through the following equation.

$$\begin{aligned}\Delta G &= G(CH_3CH_2OH@cluster) + G(e^{-}) + G(H^{+}) - G(CH_3CH_2OH@cluster) - eU - \Delta G_{H+}(pH)\\ &= G(CH_3CH_2OH@cluster) + G(1/2H_2) - G(CH_3CH_2OH@cluster) - eU - \Delta G_{H+}(pH) \qquad (3)\end{aligned}$$

Where @cluster indicates the adsorption site on the cluster; ΔG is the Gibbs free energy change considering the working condition of the elementary step; e is the elementary charge; U is the potential measured against normal hydrogen electrode at standard conditions (298.15K, 1 bar, pH=0); $\Delta G_{H+}(pH)$ is the free energy change of the protons relative to the above specified electrode at non-zero pH.[S9] In this work, U equals to 0. $\Delta G_{H+}(pH)$ equals to $-k_BT\ln(10) \times pH$, where k_B is the Boltzmann's constant and the experimental pH of this work is 8.2.

3. Supporting Figures and Tables

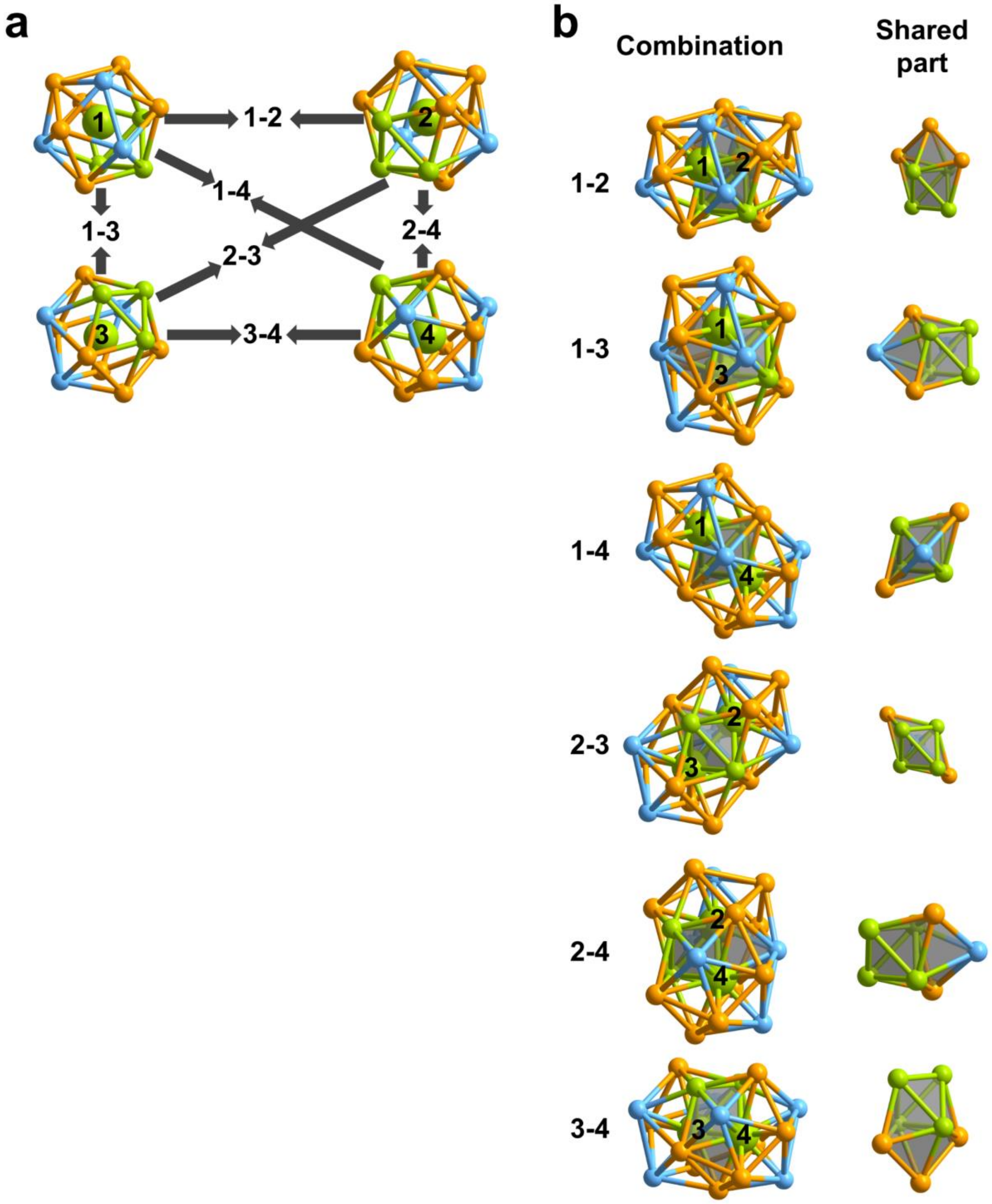

Fig. S1 (a) A pairwise combination pattern of four icosahedral $Au_{10}Ag_3$ building blocks in $Au_{18}Ag_8$ kernel of $Au_{30}Ag_{12}$. (b) Pairwise combination of $Au_{10}Ag_3$ and their shared part. Color code: orange/green, Au; blue, Ag.

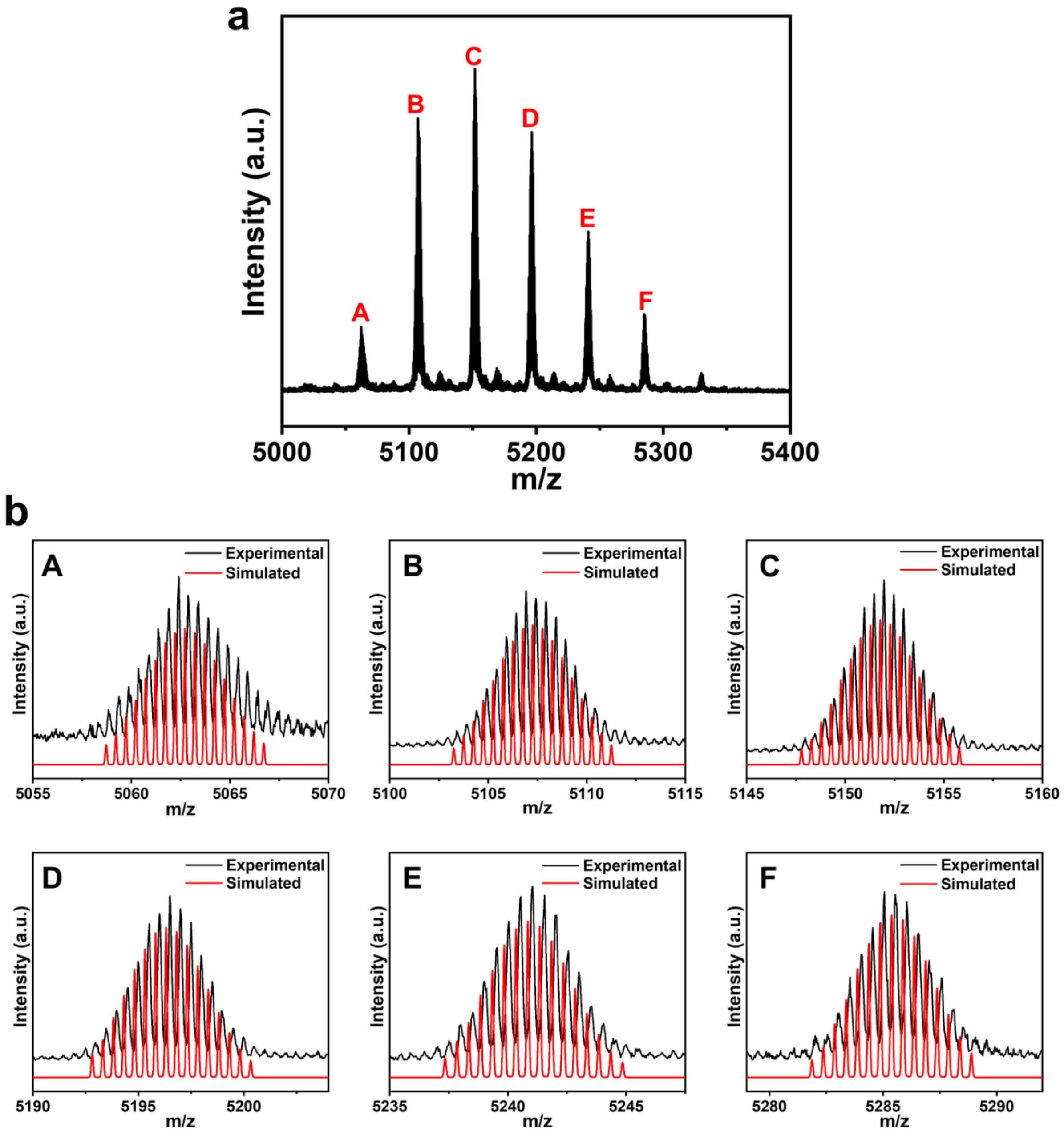

Fig. S2 (a) ESI-MS spectrum of $Au_{30}Ag_{12}(C\equiv CR)_{24}$. (b) Comparison of the experiment (black) and the simulated (red) isotopic patterns from Figure S2a: A: $[Au_{28}Ag_{14}(C_{10}H_9)_{24}\text{-}2e^-]^{2+}$; B: $[Au_{29}Ag_{13}(C_{10}H_9)_{24}\text{-}2e^-]^{2+}$; C: $[Au_{30}Ag_{12}(C_{10}H_9)_{24}\text{-}2e^-]^{2+}$; D: $[Au_{31}Ag_{11}(C_{10}H_9)_{24}\text{-}2e^-]^{2+}$; E: $[Au_{32}Ag_{10}(C_{10}H_9)_{24}\text{-}2e^-]^{2+}$; F: $[Au_{33}Ag_9(C_{10}H_9)_{24}\text{-}2e^-]^{2+}$.

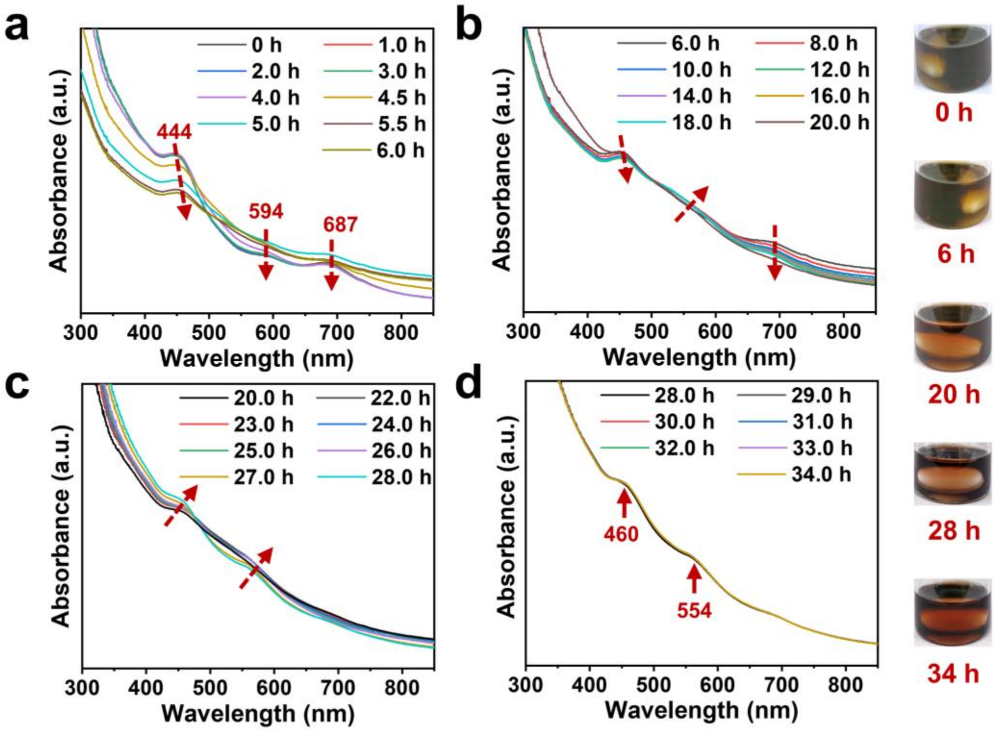

Fig. S3 Time-resolved UV-vis spectra and the photographs in details obtained from the conversion from $Au_{30}Ag_{12}(C{\equiv}CR)_{24}$ to $Au_{47}Ag_{19}(C{\equiv}CR)_{32}$ in the presence of $C_4H_{11}NBH_3$ in CH_2Cl_2.

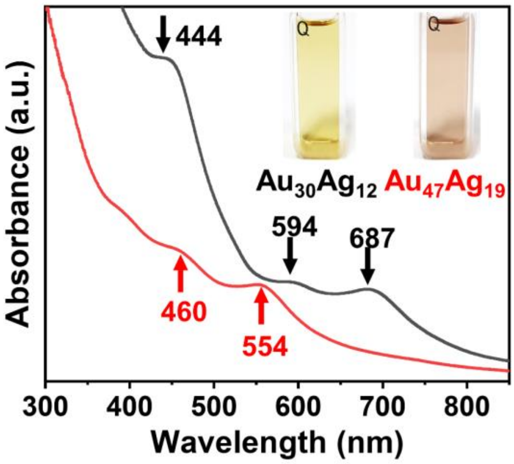

Fig. S4 UV-vis spectra and the photographs of the $Au_{30}Ag_{12}(C{\equiv}CR)_{24}$ and $Au_{47}Ag_{19}(C{\equiv}CR)_{32}$ clusters.

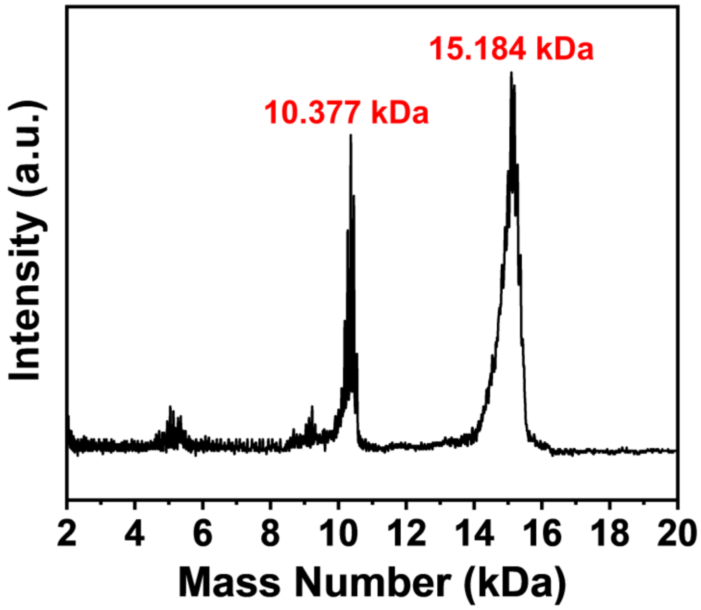

Fig. S5 MALDI-TOF-MS spectrum in the positive-ion mode of $Au_{47}Ag_{19}(C{\equiv}CR)_{32}$.

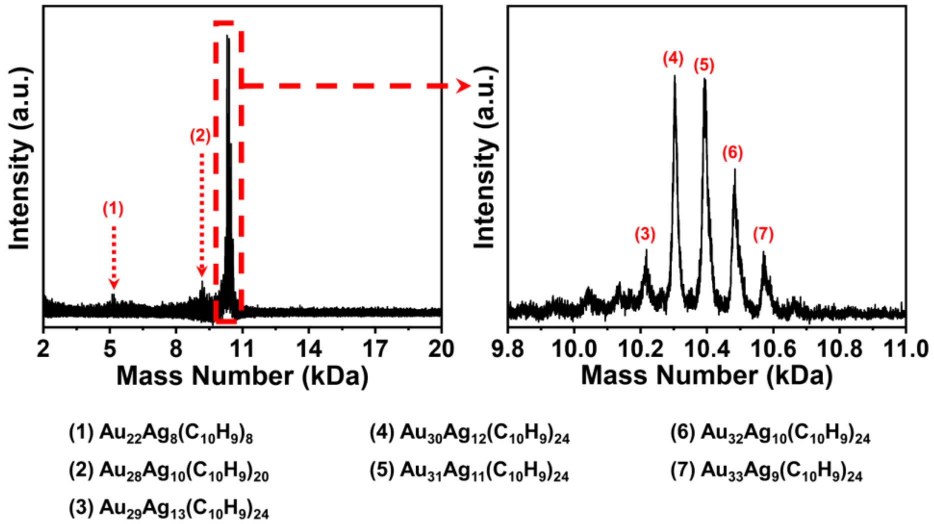

Fig. S6 MALDI-TOF-MS profiles obtained from the conversion from $Au_{30}Ag_{12}$ to $Au_{47}Ag_{19}$ at 0 h.

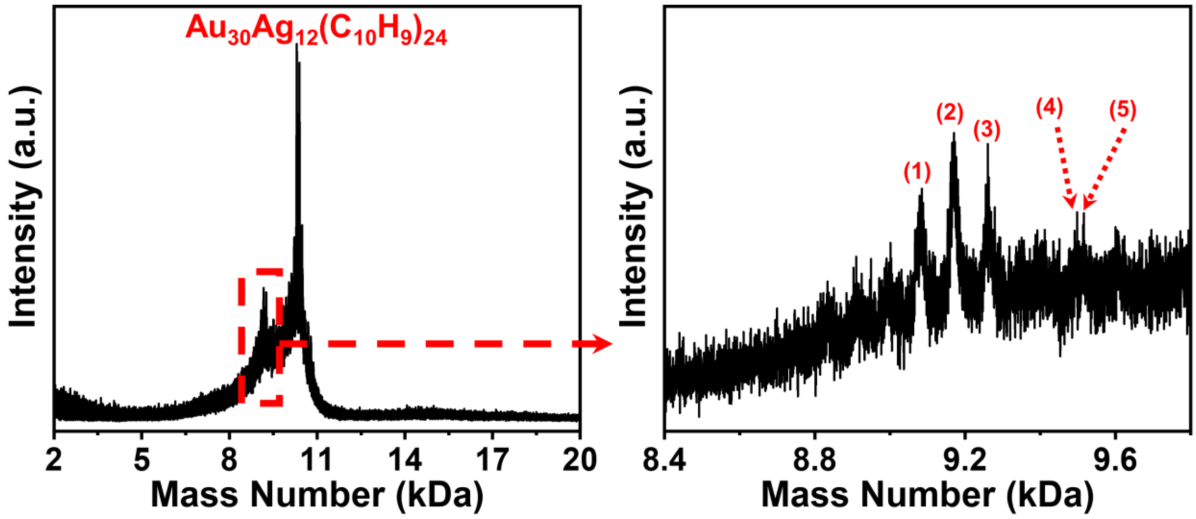

(1) $Au_{27}Ag_{11}(C_{10}H_9)_{20}$

(2) $Au_{28}Ag_{10}(C_{10}H_9)_{20}$

(3) $Au_{29}Ag_{9}(C_{10}H_9)_{20}$

(4) $Au_{29}Ag_{11}(C_{10}H_9)_{20}$

(5) $Au_{28}Ag_{12}(C_{10}H_9)_{21}$

Fig. S7 MALDI-TOF-MS profiles obtained from the conversion from $Au_{30}Ag_{12}$ to $Au_{47}Ag_{19}$ at 6 h.

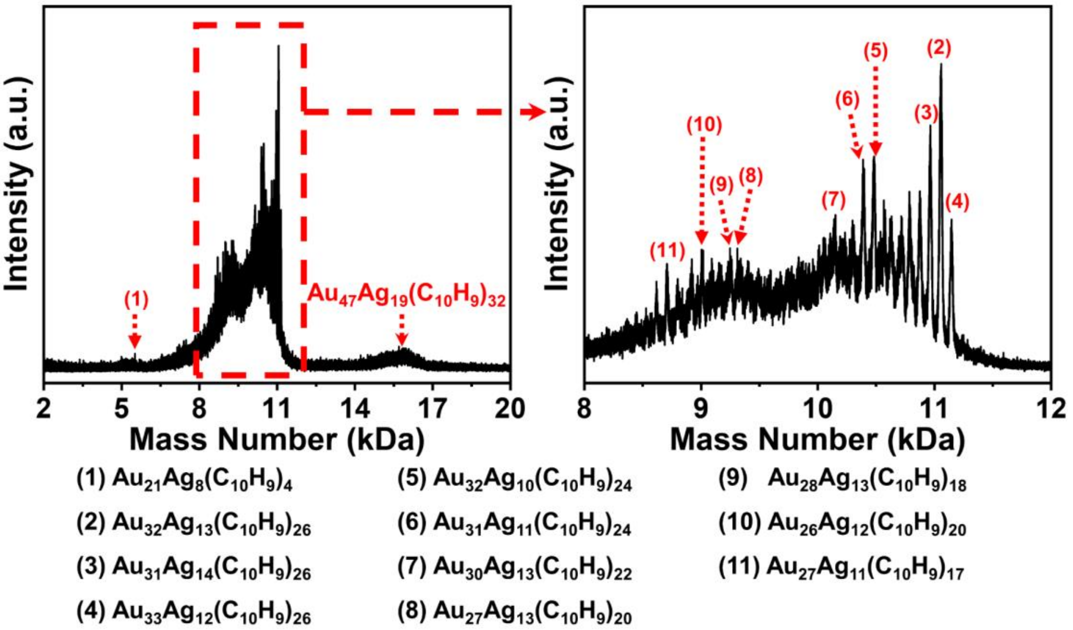

Fig. S8 MALDI-TOF-MS profiles obtained from the conversion from $Au_{30}Ag_{12}$ to $Au_{47}Ag_{19}$ at 20 h.

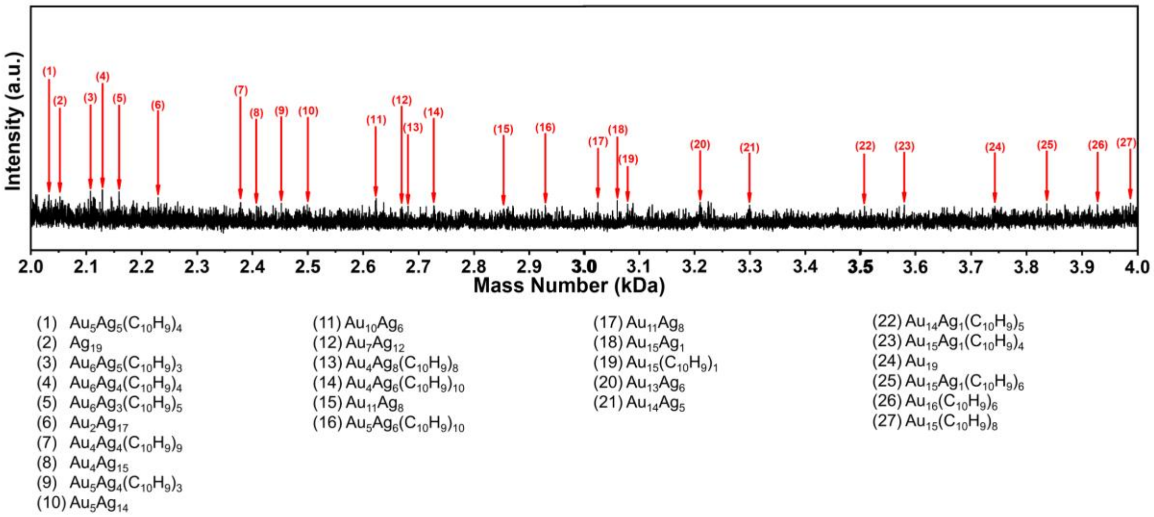

Fig. S9 MALDI-TOF-MS profiles from 2.0 kDa to 4.0 kDa obtained from the conversion from $Au_{30}Ag_{12}$ to $Au_{47}Ag_{19}$ at 28 h.

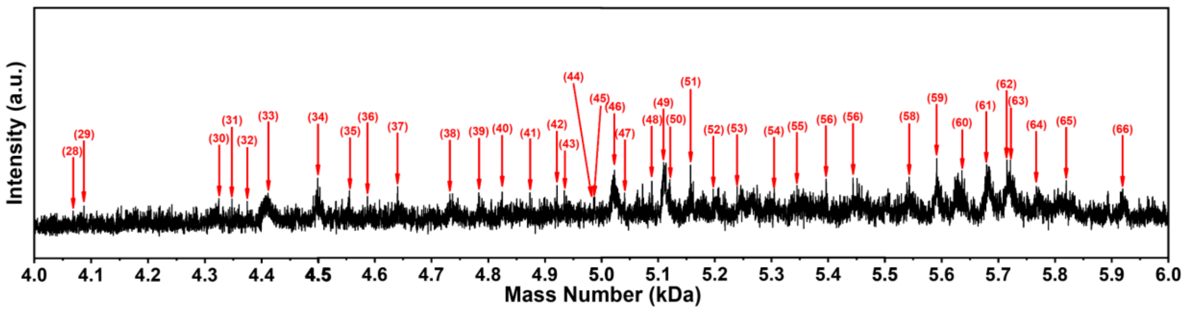

(28) $Au_8Ag_4(C_{10}H_9)_{16}$
(29) $Au_8Ag_3(C_{10}H_9)_{17}$
(30) $Au_8Ag_4(C_{10}H_9)_{18}$
(31) $Au_8Ag_3(C_{10}H_9)_{19}$
(32) $Au_8Ag_2(C_{10}H_9)_{20}$
(33) $Au_{18}Ag_8$
(34) $Au_{19}Ag_7$

(35) $Au_{19}Ag_4(C_{10}H_9)_3$
(36) $Au_{20}Ag_6$
(37) $Au_{19}Ag_6(C_{10}H_9)_2$
(38) $Au_7Ag_6(C_{10}H_9)_{21}$
(39) $Au_8Ag_7(C_{10}H_9)_{19}$
(40) $Au_8Ag_5(C_{10}H_9)_{21}$
(41) $Au_9Ag_6(C_{10}H_9)_{19}$
(42) $Au_{10}Ag_7(C_{10}H_9)_{17}$
(43) $Au_{20}Ag_8(C_{10}H_9)_1$
(44) $Au_{22}Ag_6$
(45) $Au_{11}Ag_7(C_{10}H_9)_{16}$

(46) $Au_{21}Ag_7(C_{10}H_9)_1$
(47) $Au_{21}Ag_6(C_{10}H_9)_2$
(48) $Au_{22}Ag_7$
(49) $Au_{22}Ag_6(C_{10}H_9)_1$
(50) $Au_{20}Ag_5(C_{10}H_9)_5$
(51) $Au_{21}Ag_7(C_{10}H_9)_2$
(52) $Au_{22}Ag_8$
(53) $Au_{22}Ag_6(C_{10}H_9)_2$
(54) $Au_{22}Ag_3(C_{10}H_9)_5$
(55) $Au_{22}Ag_1(C_{10}H_9)_7$
(56) $Au_{23}Ag_2(C_{10}H_9)_5$
(57) $Au_{11}Ag_{10}(C_{10}H_9)_{17}$

(58) $Au_{23}Ag_7(C_{10}H_9)_2$
(59) $Au_{24}Ag_8$
(60) $Au_{24}Ag_6(C_{10}H_9)_2$
(61) $Au_{24}Ag_4(C_{10}H_9)_4$
(62) $Au_{22}Ag_8(C_{10}H_9)_4$
(63) $Au_{11}Ag_9(C_{10}H_9)_{20}$
(64) $Au_{25}Ag_3(C_{10}H_9)_4$
(65) $Au_{26}Ag_4(C_{10}H_9)_2$
(66) $Au_{13}Ag_{12}(C_{10}H_9)_{16}$

Fig. S10 MALDI-TOF-MS profiles from 4.0 kDa to 6.0 kDa obtained from the conversion from $Au_{30}Ag_{12}$ to $Au_{47}Ag_{19}$ at 28 h.

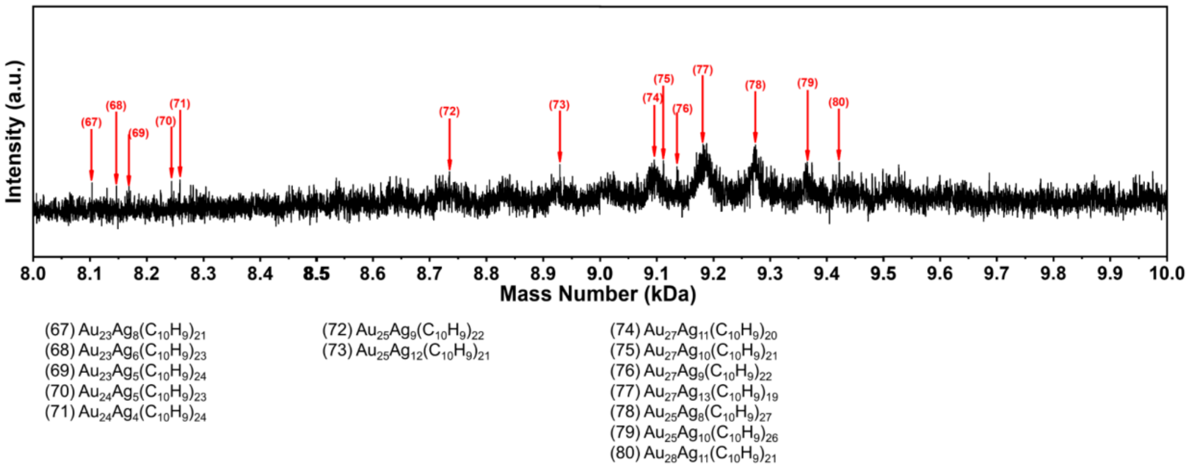

Fig. S11 MALDI-TOF-MS profiles from 8.0 kDa to 10.0 kDa obtained from the conversion from $Au_{30}Ag_{12}$ to $Au_{47}Ag_{19}$ at 28 h.

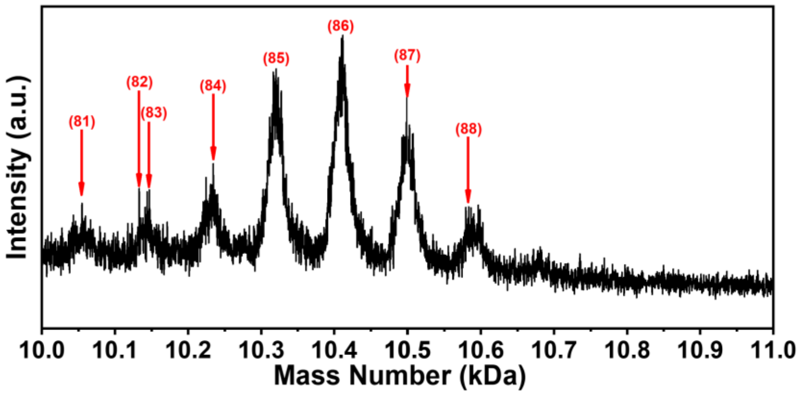

(81) $Au_{26}Ag_{17}(C_{10}H_9)_{24}$
(82) $Au_{28}Ag_{14}(C_{10}H_9)_{24}$
(83) $Au_{27}Ag_{16}(C_{10}H_9)_{24}$
(84) $Au_{28}Ag_{15}(C_{10}H_9)_{24}$
(85) $Au_{29}Ag_{14}(C_{10}H_9)_{24}$
(86) $Au_{30}Ag_{13}(C_{10}H_9)_{24}$
(87) $Au_{28}Ag_{11}(C_{10}H_9)_{21}$
(88) $Au_{32}Ag_{11}(C_{10}H_9)_{24}$

Fig. S12 MALDI-TOF-MS profiles from 10.0 kDa to 11.0 kDa obtained from the conversion from $Au_{30}Ag_{12}$ to $Au_{47}Ag_{19}$ at 28 h.

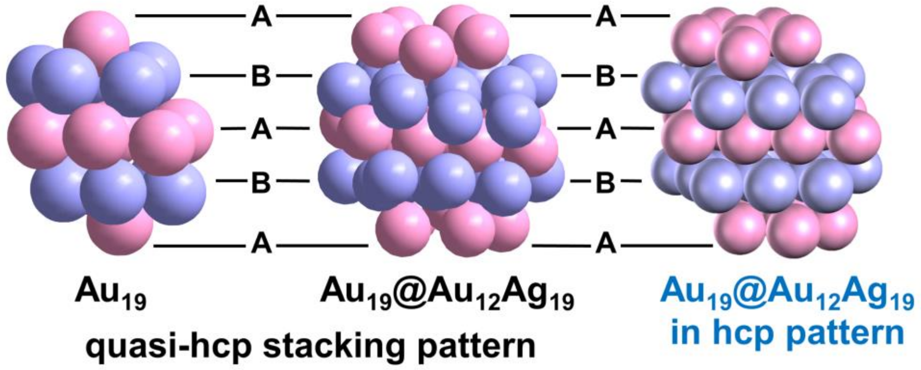

Fig. S13 Au_{19} and $Au_{19}@Au_{12}Ag_{19}$ in quasi-hcp structure stacking in ABABA pattern. Color codes: green, Au; pink/ purple, Au/Ag.

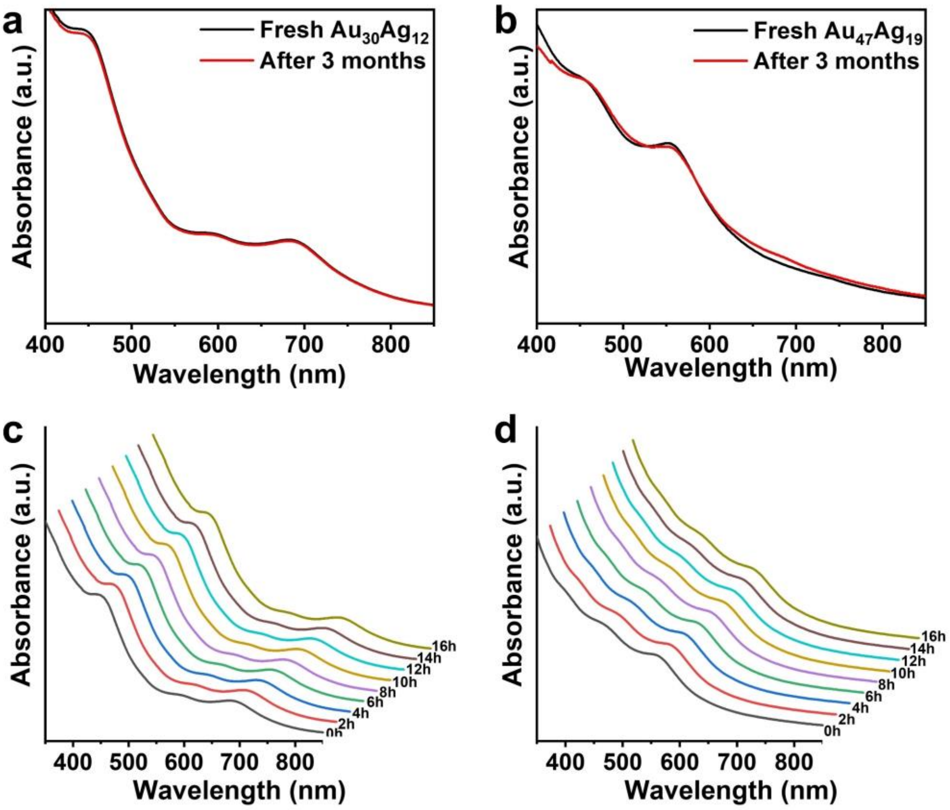

Fig. S14 UV-vis spectra of (a) $Au_{30}Ag_{12}$ and (b) $Au_{47}Ag_{19}$ in solid state stored under ambient conditions for three months. UV-vis spectra of (c) $Au_{30}Ag_{12}$ and (d) $Au_{47}Ag_{19}$ in toluene solution at 70°C for 16 h.

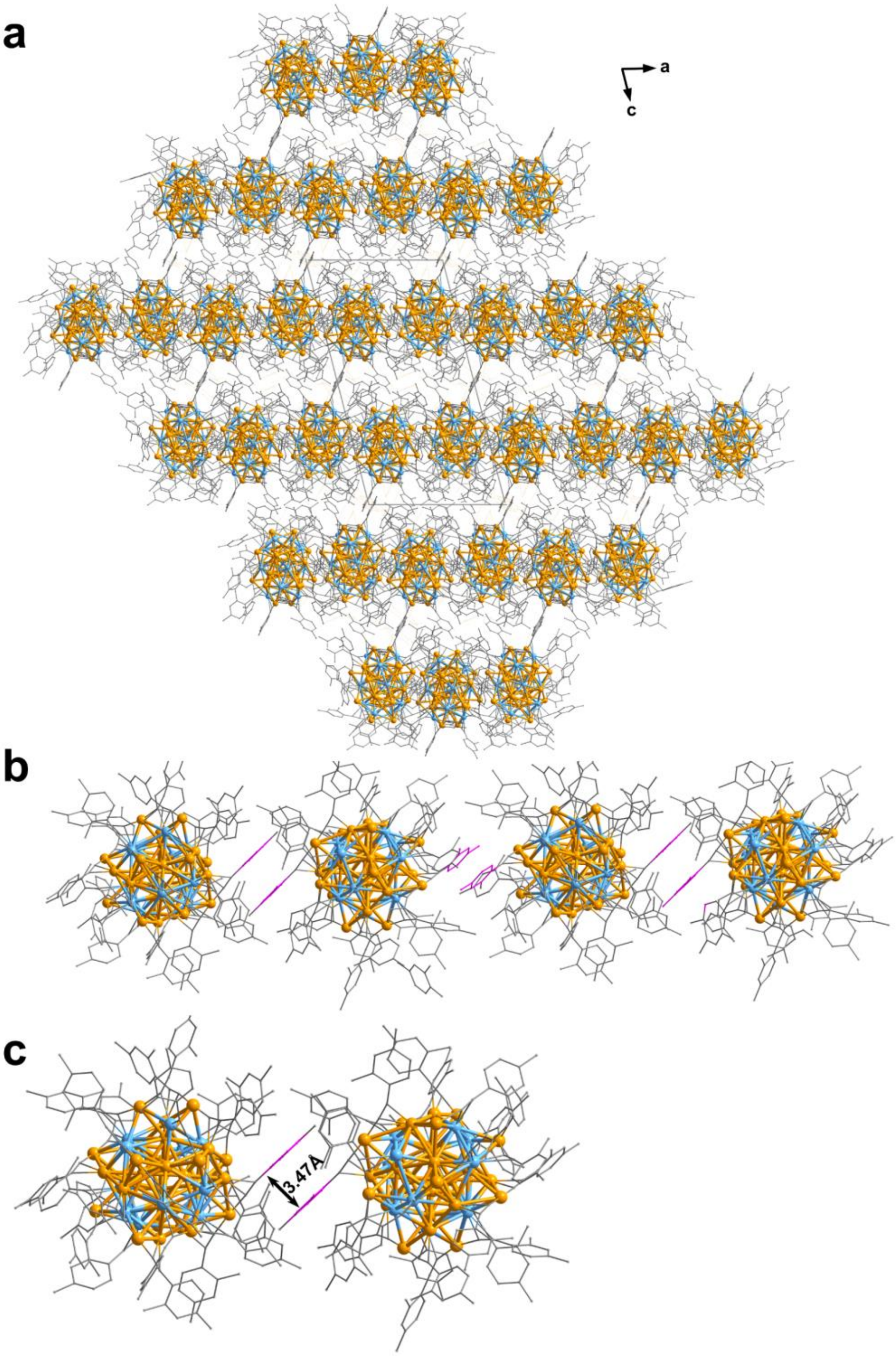

Fig. S15 $Au_{30}Ag_{12}$ cluster in-lattice connection mode: (a) in-lattice linear assembly; (b) $Au_{30}Ag_{12}$ assembly mode local amplification; (c) π-π conjugation between clusters. Color code: orange, Au; blue, Ag; gray, C. The H atoms are omitted for clarity.

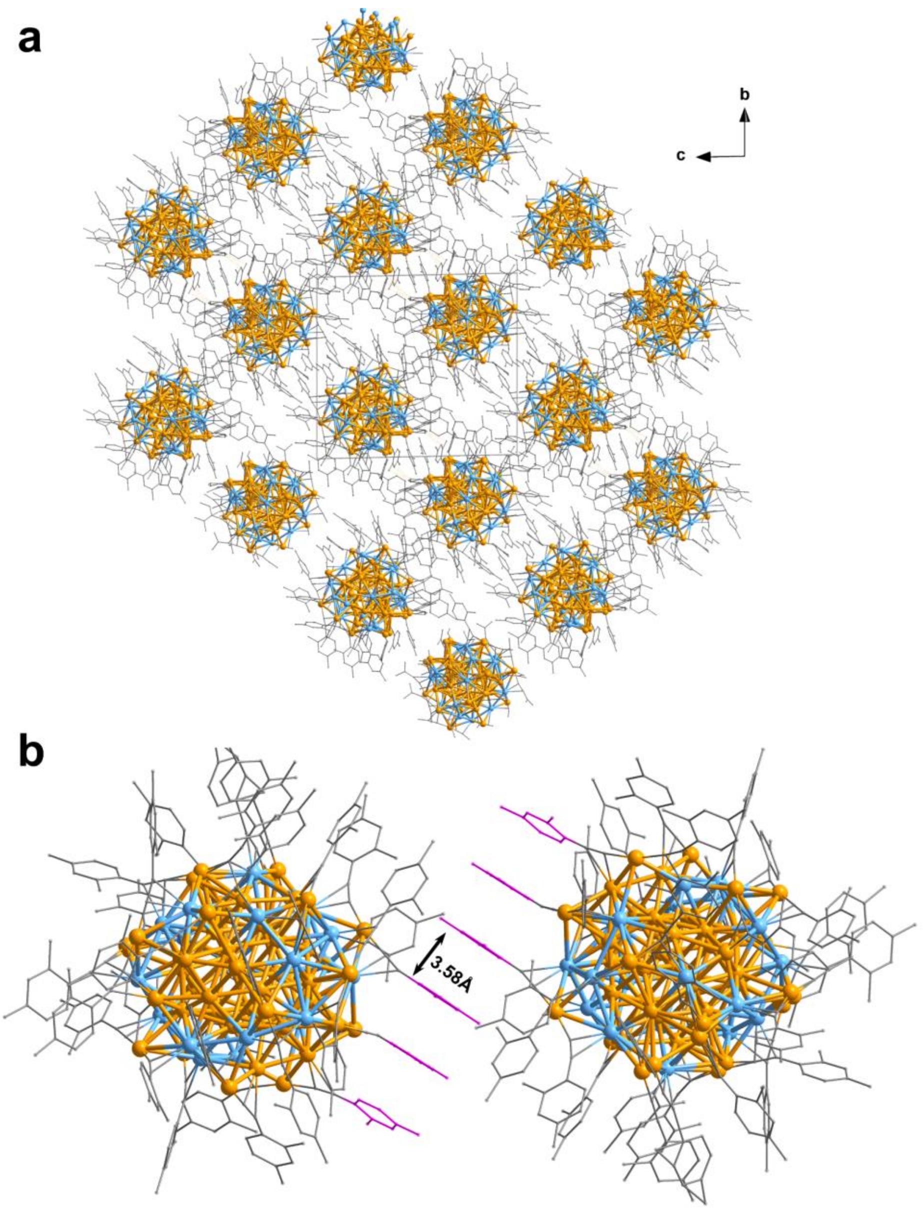

Fig. S16 $Au_{47}Ag_{19}$ cluster in-lattice connection mode: (a) in-lattice linear assembly; (b) $Au_{47}Ag_{19}$ assembly mode local amplification and π-π conjugation between clusters. Color code: orange, Au; blue, Ag; gray, C. The H atoms are omitted for clarity.

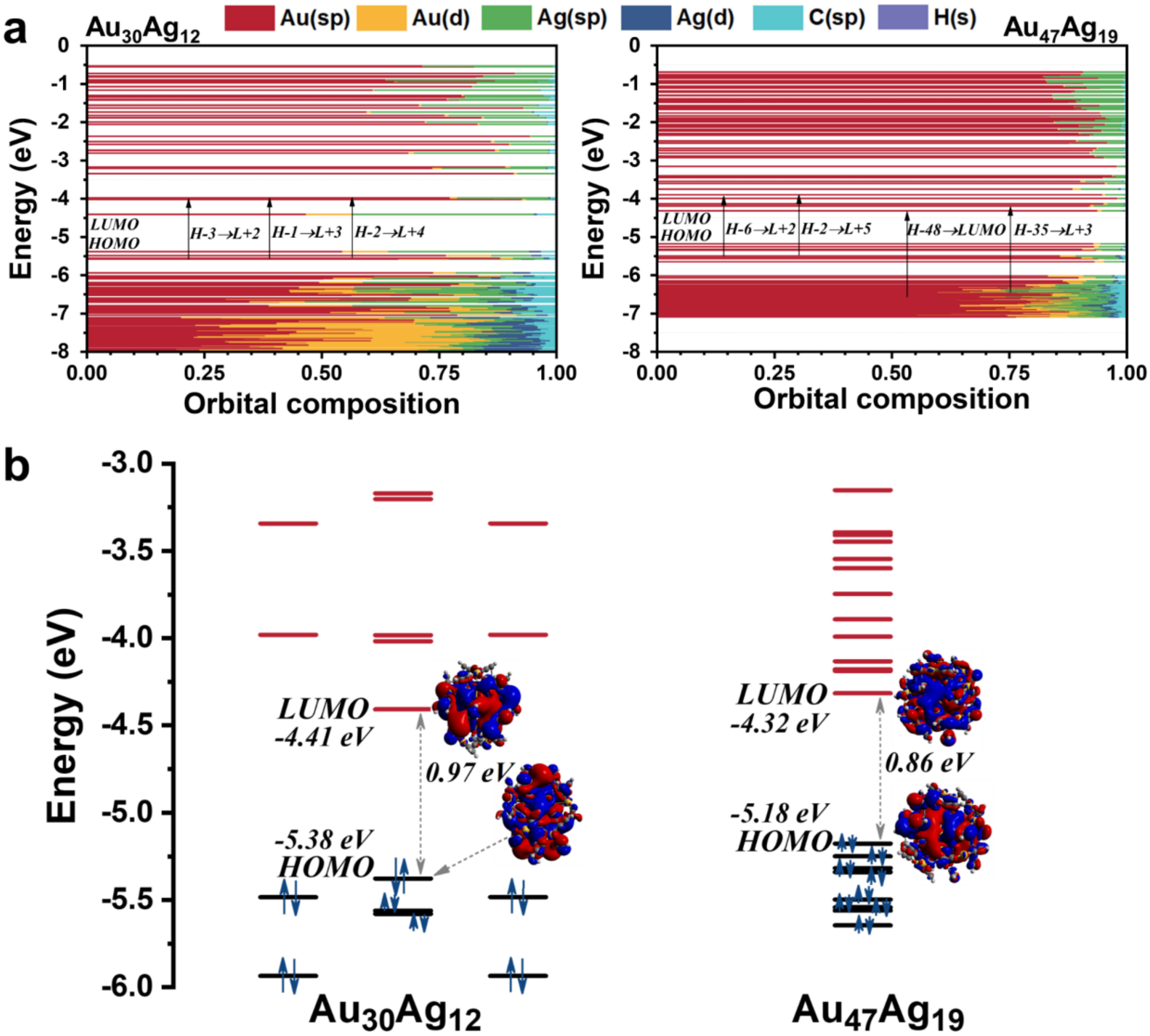

Fig. S17 (a) KS orbital energy level diagram for $Au_{30}Ag_{12}$ (left) and $Au_{47}Ag_{19}$ (right) clusters with contributions from various atomic-orbitals of Au, Ag, C and H. (b) Energies and the molecular orbital topologies (Iso: 0.005) of HOMO and LUMO orbitals.

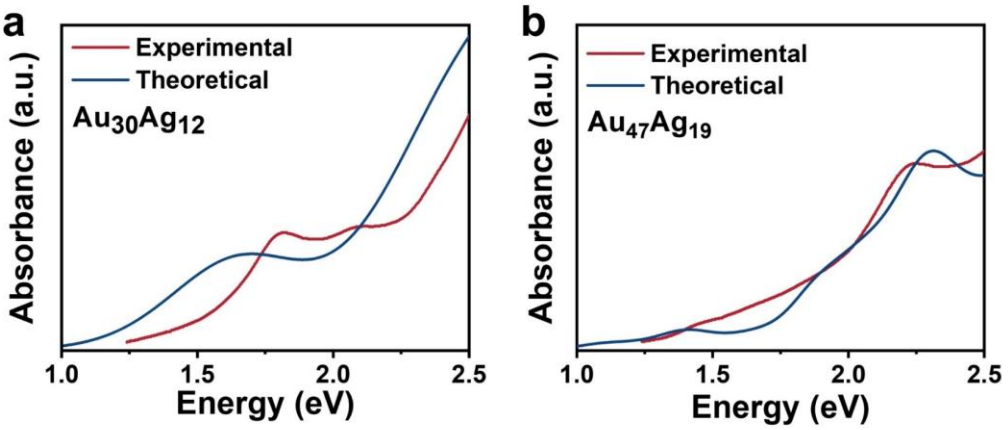

Fig. S18 Experimental and theoretical absorption spectra for (a) $Au_{30}Ag_{12}$ and (b) $Au_{47}Ag_{19}$.

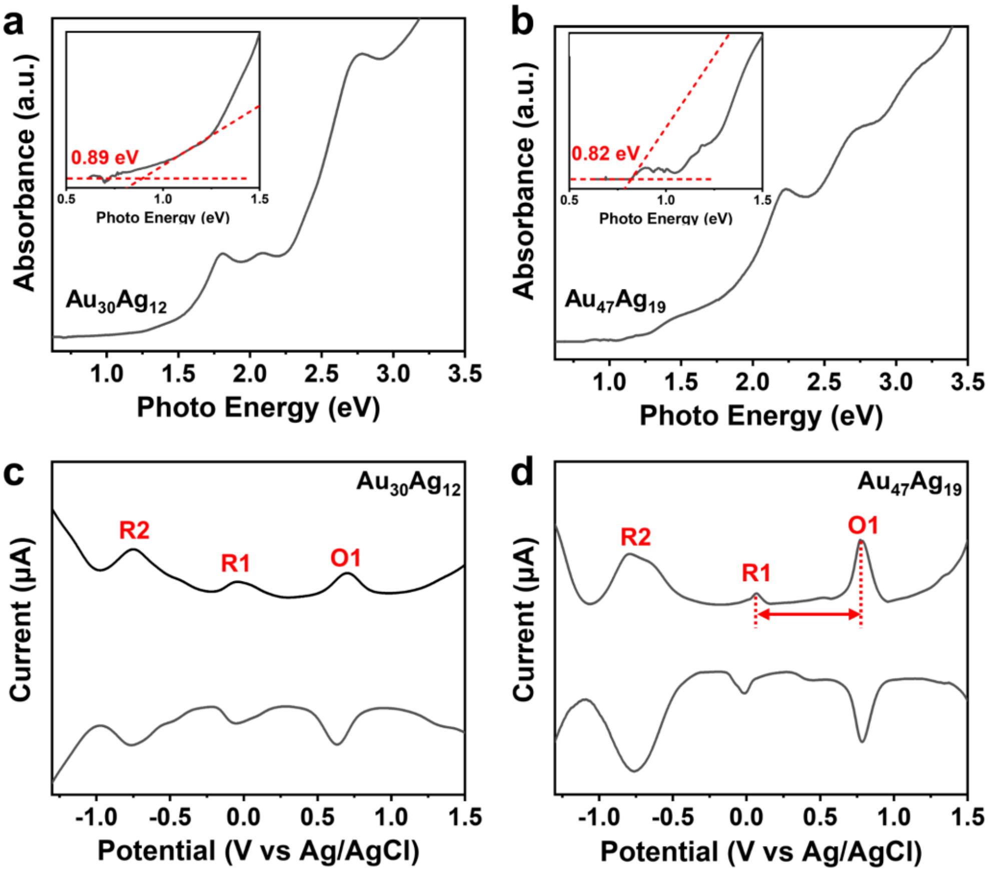

Fig. S19 UV−vis−NIR absorption spectra in the photon energy scale of (a) $Au_{30}Ag_{12}$ and (b) $Au_{47}Ag_{19}$. Square wave voltammetry curves of (c) $Au_{30}Ag_{12}$ and (d) $Au_{47}Ag_{19}$.

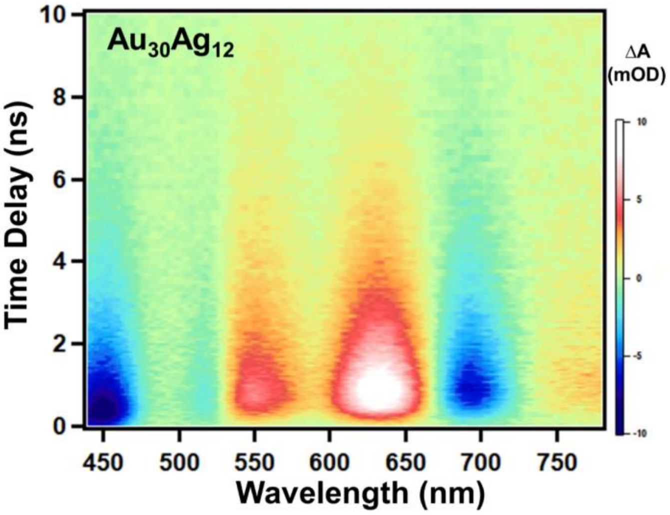

Fig. S20 Nanosecond TA data map of $Au_{30}Ag_{12}$ with excitation of 400 nm.

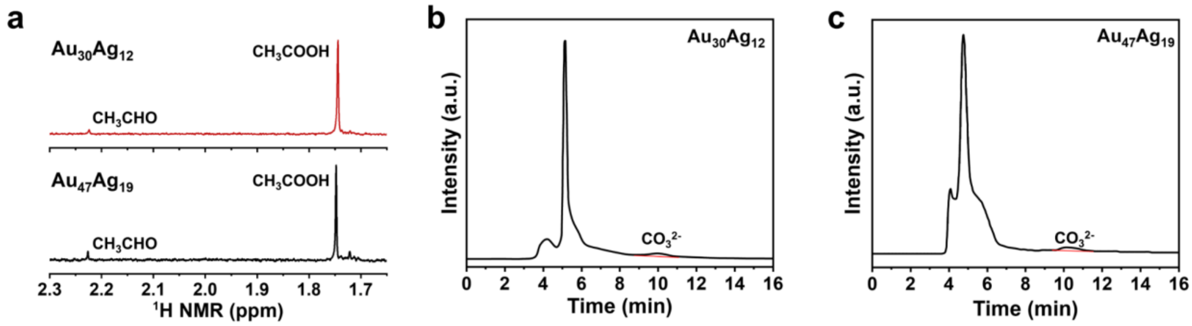

Fig. S21 (a) ^{1}H NMR chemical shifts obtained from the liquid products of EOR reactions. Ion chromatography analysis obtained from CO_3^{2-} in the electrolyte solution after the EOR reaction over the (b) $Au_{30}Ag_{12}$ and (c) $Au_{47}Ag_{19}$ catalysts.

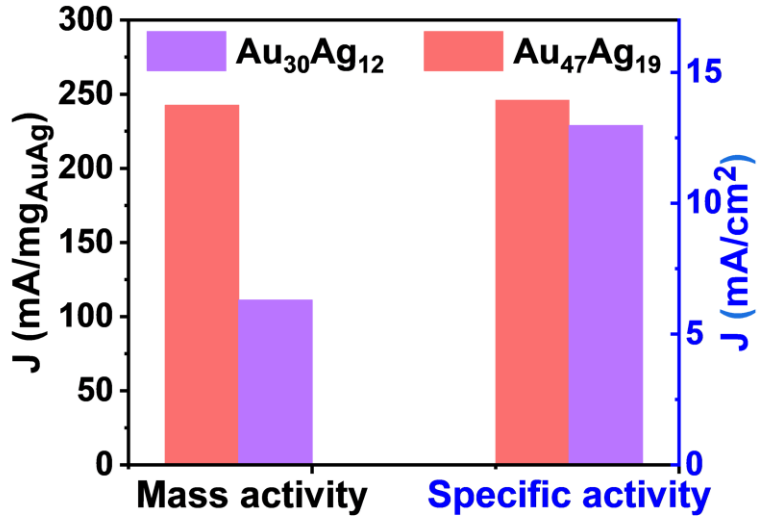

Fig. S22 Specific and mass activities of the two catalysts toward EOR at 0.08 V vs Ag/AgCl.

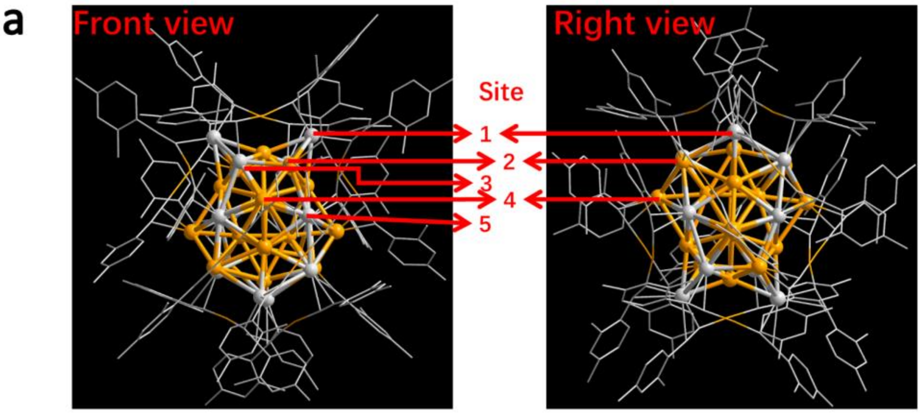

Site	Relative Energy /eV	Site	Relative Energy /eV
1	1.02	**4**	1.00
2	1.11	**5**	0.95
3	0.99		

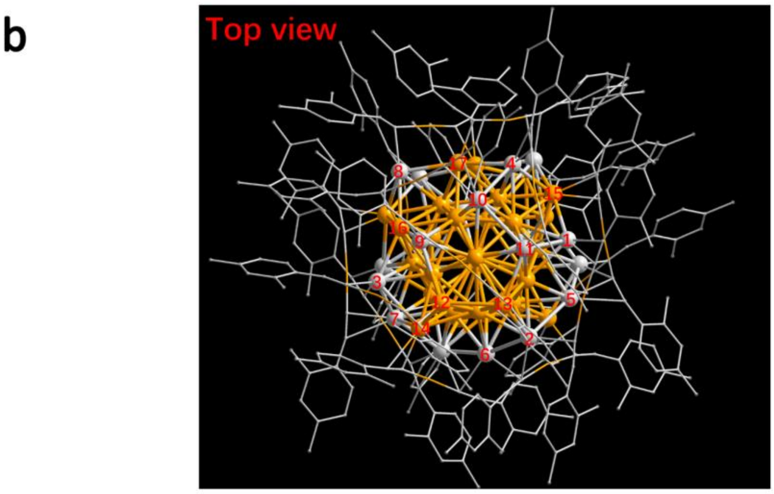

Site	Relative energy /eV	Site	Relative energy /eV
1	0.97	10	1.39
2	0.91	11	1.34
3	1.11	12	1.56
4	1.06	13	1.48
5	1.01	14	0.83
6	0.76	15	1.10
7	1.16	16	1.06
8	1.03	17	0.88
9	1.27		

Fig. S23 Possible reactive sites on (a) $Au_{30}Ag_{12}$ and (b) $Au_{47}Ag_{19}$ clusters. Relative energy indicates the change of the electronic energy of the reaction step with the largest Gibbs free energy change, i.e. $E(*CH_3CH_2O) + E(1/2H_2) - E(*CH_3CH_2OH)$, which is used to screen the reactive sites with reduced computational price.

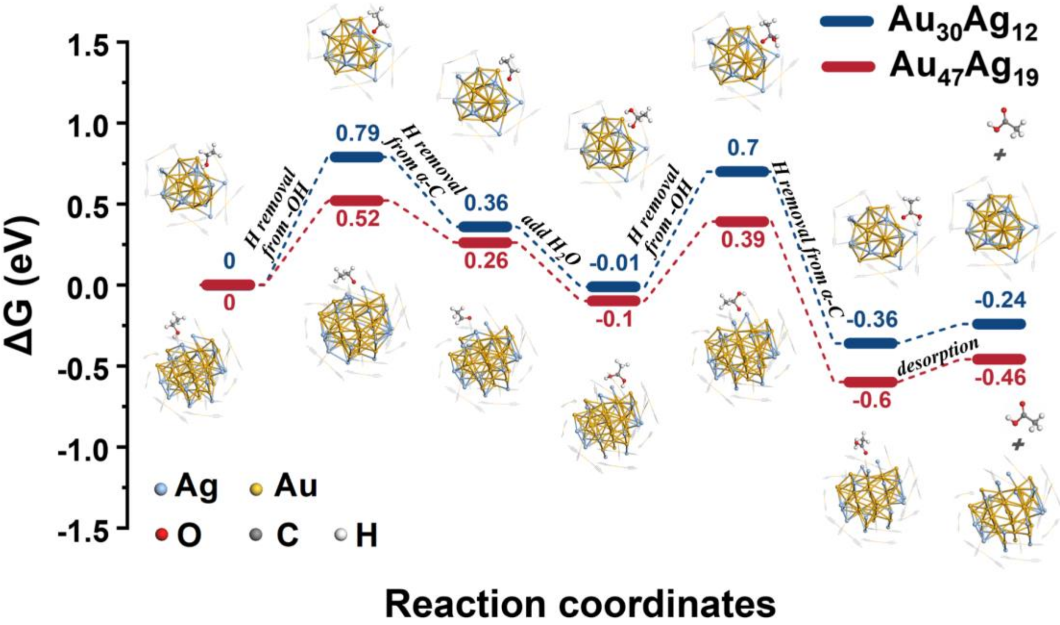

Fig. S24 Gibbs free energy diagrams of the oxidation reaction from CH_3CH_2OH to CH_3COOH catalyzed by the $Au_{30}Ag_{12}$ and $Au_{47}Ag_{19}$ clusters.

Table S1. Crystal data and structure refinement for the $Au_{30}Ag_{12}(C\equiv CR)_{24}$ cluster.

Empirical formula	C470H423Ag24Au60	
Formula weight	20477.93	
Temperature	296(2) K	
Wavelength	0.71073 Å	
Crystal system	Triclinic	
Space group	P-1	
Unit cell dimensions	a = 21.3484(14) Å	α = 79.7870(10)°
	b = 29.2299(19) Å	β = 75.6320(10)°
	c = 40.094(3) Å	γ = 89.0660(10)°
Volume	23842(3) $Å^3$	
Z	2	
Density (calculated)	2.852 mg/m^3	
Absorption coefficient	19.377 mm^{-1}	
F(000)	18222	
Theta range for data collection	2.2855 to 27.0745°	
Index ranges	-25<=h<=22, -35<=k<=35, -48<=l<=47	
Reflections collected	151246	
Independent reflections	84875 [R(int) = 0.0484]	
Completeness to theta = 25.242°	97.2 %	
Absorption correction	Multi-Scan	
Refinement program	SHELXL-2018/3(Sheldrick,2018)	
Data / restraints / parameters	84875 / 33478 / 4744	
Goodness-of-fit on F^2	1.190	
Δ/σ_{max}	0.009	
Final R indices [I>2sigma(I)]	R1 = 0.0809, wR2 = 0.2010	
R indices (all data)	R1 = 0.1451, wR2 = 0.2650	
Largest diff. peak and hole	5.045 and -5.534 $eÅ^{-3}$	

Table S2. Crystal data and structure refinement for the $Au_{47}Ag_{19}(C{\equiv}CR)_{32}$ cluster.

Empirical formula	C320H290Ag19Au47	
Formula weight	15442.46	
Temperature	296(2) K	
Wavelength	0.71073 Å	
Crystal system	Triclinic	
Space group	P-1	
Unit cell dimensions	a = 23.0809(5) Å	α = 91.0290(10)°
	b = 25.7505(6) Å	β = 94.2840(10)°
	c = 28.4251(7) Å	γ = 92.4620(10)°
Volume	16827.8(7) Å^3	
Z	2	
Density (calculated)	3.048 mg/m^3	
Absorption coefficient	21.510 mm^{-1}	
F(000)	13632	
Theta range for data collection	1.946 to 25.520°	
Index ranges	-27<=h<=27, -31<=k<=31, -29<=l<=34	
Reflections collected	135857	
Independent reflections	62319 [R(int) = 0.0592]	
Completeness to theta = 25.242°	99.6 %	
Absorption correction	Multi-Scan	
Refinement program	SHELXL-2018/3(Sheldrick,2018)	
Data / restraints / parameters	62319 / 22435 / 3571	
Goodness-of-fit on F^2	1.071	
Δ/σ_{max}	0.003	
Final R indices [I>2sigma(I)]	R1 = 0.0669, wR2 = 0.1927	
R indices (all data)	R1 = 0.1234, wR2 = 0.2251	
Largest diff. peak and hole	3.149 and -5.297 eÅ^{-3}	

Table S3. Fitting parameters of TA kinetics of the two clusters probed at 630 nm.

	$Au_{30}Ag_{12}$	$Au_{47}Ag_{19}$
τ_1	0.5 ps (19)	0.5 ps (-33)
τ_2	0.8 ps (-17.6)	0.9 ps (23)
τ_3	2.5 ns (14.7)	0.4 ns (5.9)
τ_4		1.8 ns (3.4)

4. Supporting references

(S1) M. Frisch, G. Trucks, H. Schlegel, G. Scuseria, M. Robb, J. Cheeseman, G. Scalmani, V. Barone, B. Mennucci, G. Petersson, Gaussian 09, Rev. D. 01. 2009.

(S2) F. Neese, F. Wennmohs, U. Becker and C. Riplinger, *J. Chem. Phys*., 2020, **152**, 224108.

(S3) M. Wergifosse and S. Grimme, *J. Chem. Phys*., 2018, **149**, 024108.

(S4) M. Bajdich, M. García-Mota, A. Vojvodic, J. Nørskov and A. Bell, *J. Am. Chem. Soc.*, 2013, **135**, 13521-13530.